EES Solar

Accepted Manuscript

This article can be cited before page numbers have been issued, to do this please use: H. Yan, Y. Cui and W. Ma, *EES Sol.*, 2026, DOI: 10.1039/D5EL00160A.

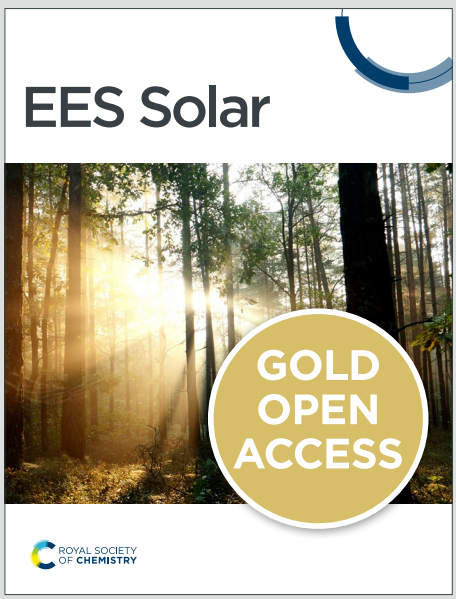

View Article Online
DOI: 10.1039/D5EL00160A

The development of organic photovoltaics (OPVs) has long-term relied on iterative, experience-based experimentation, limiting the speed and scalability of innovation. Despite impressive advances in power conversion efficiency (PCE), the discovery of new materials and optimization of device performance remain hindered by fragmented data and a lack of systematic knowledge integration. Here, we introduce an Intelligent Data-Driven Framework (IDDF) that unifies large language models, high-throughput quantum chemical calculations, and explainable machine learning to transform OPV research into a data-driven discipline. By extracting structured knowledge from 615 scientific papers and combining it with a comprehensive quantum-chemical dataset, AIRS establishes quantitative structure–performance relationships (QMSPR) that guide molecular design with unprecedented interpretability and accuracy. This work represents a paradigm shift—not only for OPV, but for materials science at large—by demonstrating how artificial intelligence can automate knowledge synthesis and predictive modeling in complex scientific domains. As the fully integrated AI system tailored for OPV, our approach accelerates discovery, reduces reliance on trial-and-error, and unlocks the hidden value of decades of published research. It exemplifies the future of intelligent scientific infrastructure, where AI acts as a co-researcher, enabling sustainable energy technologies to advance with greater speed, transparency, and reproducibility.

View Article Online
DOI: 10.1039/D5EL00160A

ARTICLE

Developing An Intelligent Data-Driven Framework for Organic Photovoltaic Research†

Received 00th January 20xx,
Accepted 00th January 20xx

DOI: 10.1039/x0xx00000x

Yu Cui, [a] Wei Ma, [a] and Han Yan *[a]

The current trial-and-error research paradigm is inherently inappropriate for organic photovoltaic (OPV) development as a result of its diverse photovoltaic materials together with sophisticated device fabrication conditions. A data-driven paradigm is therefore particularly well-suited to address these challenges. The data-driven research paradigm requires big-data extraction from literatures, high-throughput quantum chemical calculation according to chemical structures, and quantitative molecular structure-property relationship (QMSPR). To address these, we develop an Intelligent Data-Driven Framework (IDDF) leveraging large language models (LLMs), high-throughput quantum chemistry calculation platform (HQCCP), and explainable machine learning (ML). With the aid of IDDF, we extract structured data from 615 peer-reviewed articles and compute 50 molecular descriptors for 125 Y-series acceptors, forming a QMSPR database linking molecular features to device performance. Using eXtreme Gradient Boosting (XGBoost)-SHapley Additive exPlanations (SHAP) ML model, the IDDF maps molecular substructures to key descriptors and device power conversion efficiency (PCE). The results quantitatively demonstrate the influences of each building block of Y-series acceptors on final PCE values with explicit quantum chemical explanations. Our framework shifts OPV research from intuition-based design toward a knowledge-guided, predictive mode, providing a foundational step toward autonomous materials discovery and enhance the competitiveness of OPVs among emerging photovoltaic technologies.

1. Introduction

The advent of Y6 marked a breakthrough of power conversion efficiency (PCE) for organic photovoltaics (OPVs) [1]. Inspiring by its molecular design, the improved non-fullerene acceptors (NFAs) vigorously elevate the PCE from 15.7% to 21.0%.[1-7] The remarkable PCE progress has sparked global interest in OPV as a promising candidate for the next-generation photovoltaic technology.[8-10] During the past ten years, the annual number of OPV research papers has grown from 3532 to 6209 according to the Web of Science search results. However, a noticeable trend is that the pace of PCE growth has gradually slowed down due to the lack of milestone material revolution since 2019. The disconnect between research outputs and PCE growth is to some extent due to the trial-and-error experimentation research paradigm. As the OPV molecular design becomes increasingly complex, this traditional paradigm has become unsustainable, limiting both the efficacy of material discovery and its scalability. The sluggish PCE growth erodes OPVs' competitive advantage against other emerging photovoltaic techniques such as the perovskite solar cell, even in the specialized applications requiring semi-transparent and mechanically flexible properties.[9-16]

To break this impasse, a fundamental paradigm shift from empirical exploration to data-driven innovation is urgently needed. Over the past decade, the OPV field has accumulated an extensive body of literatures encompassing thousands of photovoltaic materials and their corresponding device performances, providing a solid foundation for this transformation.[10,17] However, efforts to fully unlock this knowledge potential have long been constrained due to the lack of efficient and accurate structured data extraction method. Traditional approaches relying on manual curation or rule-based information extraction are time-consuming, error-prone, and ill-suited to address the prevalent linguistic diversity and unstructured formats in academic literatures.[18-20] Recent advances in LLMs have demonstrated remarkable capabilities in scientific text comprehension, enabling high-precision, context-aware information extraction, and automated data mining.[21,22] By further integrating with optimized prompting strategies, it is feasible to extract high-quality structured device data from literatures.[23-26]

The next challenge for data-driven research lies in establishing quantitative molecular structure-property relationship (QMSPR), particularly for the Y-series NFAs those dominate the highly performed OPVs [6,7]. While ML offers a powerful tool for uncovering the hidden patterns, directly correlating molecular fingerprints or Simplified Molecular Input Line Entry System (SMILES) strings with PCE often yields scientifically limited black-box models, which are insufficient to construct QMSPR in OPVs.[27-31] Crucially, PCE is not an intrinsic molecular property but rather an outcome of multiple

[a] State Key Laboratory for Mechanical Behavior of Materials, School of Materials Science and Engineering, Xi'an Jiaotong University, Xi'an 710049, China.
E-mail: mseyanhan@xjtu.edu.cn.
† Electronic Supplementary Information (ESI) available: Details of experiments and calculations; supplementary figures, supplementary tables, and supplementary references. See DOI: 10.1039/x0xx00000x

View Article Online DOI: 10.1039/D5EL00160A

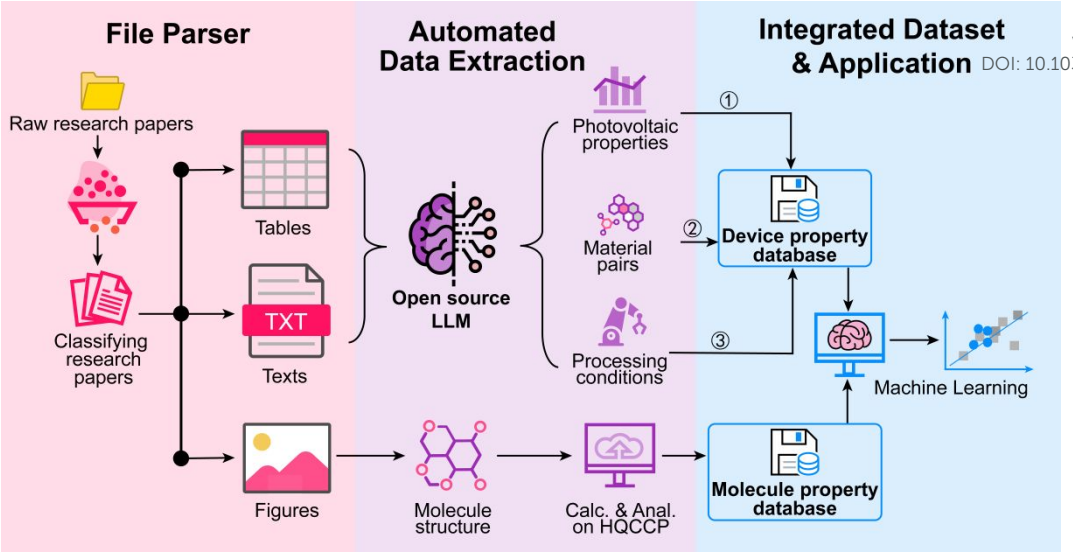

Fig. 1 Overall schematic of the IDDF.

synergistic photophysical processes dominated by the molecular properties. The significant PCE variations observed among structurally similar Y-series NFAs demonstrate how subtle molecular structure tuning can govern device performance by modulating photoelectric properties.[9,10,32,33] Thus, an effective modelling framework must decouple the complex structure-property relationship into physically meaningful molecular properties. Central to this approach is a well-defined set of molecular optoelectronic descriptors serving as physical bridges between chemical structures of photovoltaic materials and device PCEs. To enable reliable and large-scale acquisition of these descriptors, the high-throughput quantum chemical calculation with low cost is essential. After that, using the standardized datasets of Y-series molecular properties, a two-stage ML pipeline can be constructed: first, correlating computationally derived optoelectronic descriptors with experimentally extracted device PCEs to identify dominant physical parameters; second, linking molecular structures to those key descriptors to reveal how specific substructures determine optoelectronic descriptors. This hierarchical modelling strategy guarantees the data-driven innovation in OPVs.

By integrating these components, we establish an Intelligent Data-Driven Framework (IDDF) for OPVs that links molecular structure to device performance through quantifiable optoelectronic descriptors. Our approach combines LLM-assisted literature mining with a standardized high-throughput quantum chemistry computation platform (HQCCP) to construct a comprehensive structure–property–performance dataset for Y-series NFAs. This dataset includes 32 device-level parameters extracted from 615 peer-reviewed publications and 50 computed molecular descriptors for 125 representative molecules. Leveraging explainable machine learning, we quantitatively disentangle the influence of specific molecular substructures—including central electron-accepting cores, end groups, donor units, and side chains—on fundamental optoelectronic properties and, ultimately, on PCE. This analysis reveals the physical mechanisms by which molecular design dictates device performance. Our framework represents a modest yet significant stride in advancing organic photovoltaic (OPV) molecular design from empirical intuition towards a predictable and interpretable scientific domain, providing a design reference for future Y-series acceptors. It represents a critical step in shifting OPV research away from trial-and-error exploration toward knowledge-driven innovation, thereby helping to accelerate R&D cycles and enhance competitiveness among emerging photovoltaic technologies.

2. Results and discussion

2.1. Overall workflow of IDDF

The big-data collection is the prerequisite for OPV's data-driven innovation. Taking advantage of the LLM, the structured information on material pairs, device processing conditions, and photovoltaic parameters in texts and tables can be directly converted to metadata.[26,34] To obtain the missing molecular properties, we developed HQCCP to transform molecular images into strings as inputs and conducted high-throughput quantum chemical computation. Based on the two implements, the IDDF composing of File Parser, Automated Data Extraction, and Integrated Dataset & Application is proposed to construct the QMSPR in OPV (Fig. 1). The "File Parser" module first classifies the literatures, and then extracts texts, tables, and images from the classified literatures for the downstream data processing. The "Automated Data Extraction" module collects material pairs, photovoltaic parameters, and processing conditions from the contents. Additionally, it incorporates image recognition tools to convert molecular structure images into SMILES strings for following calculation. The "Integrated Dataset & Application" module performs data cleaning, validation, and alignment to merge device performance with molecular electronic property. The integrated dataset supports explainable ML analysis by XGBoost-SHAP method. This end-to-end automatic workflow enables efficient transformation from

View Article Online
DOI: 10.1039/D5EL00160A

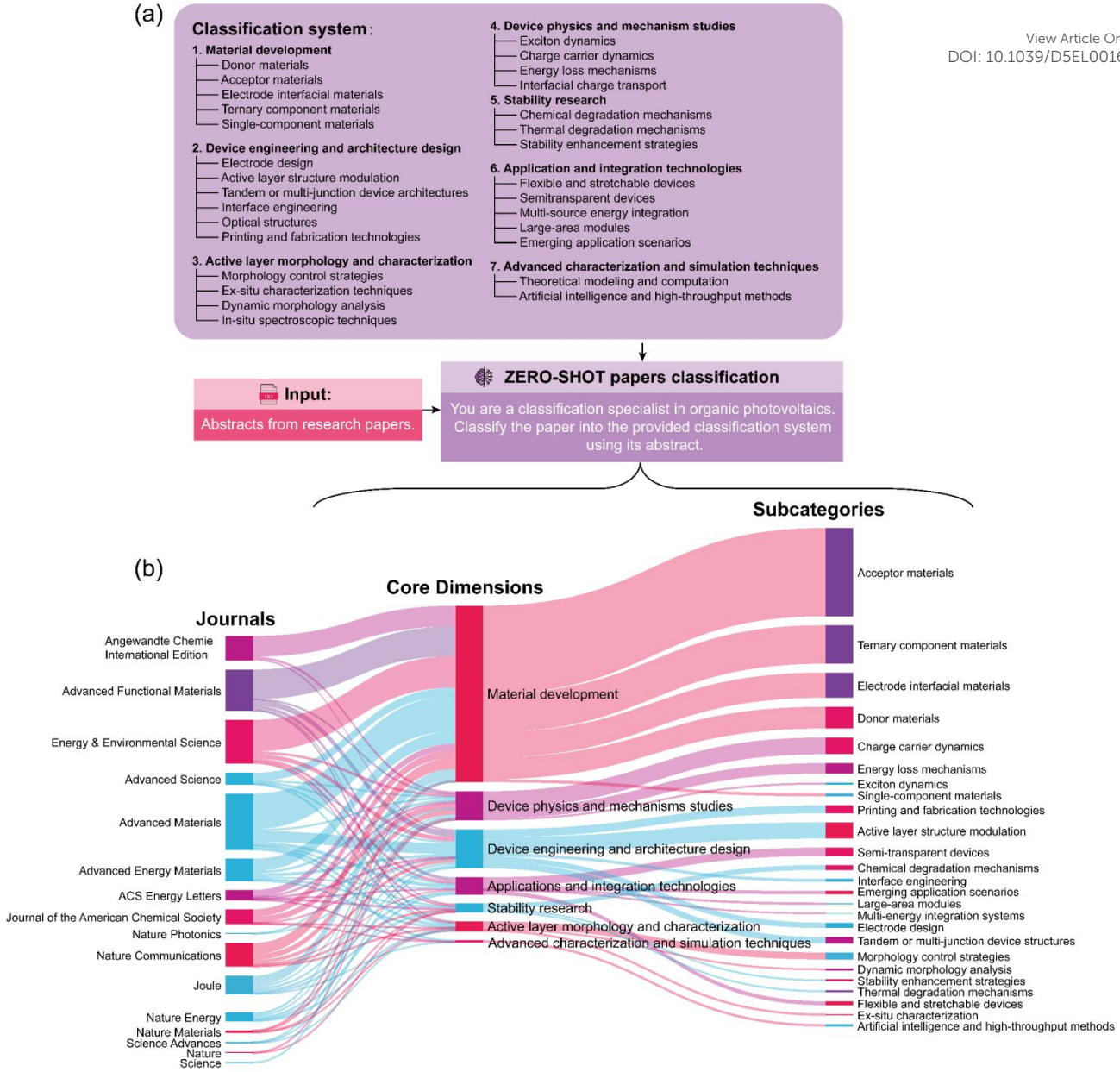

Fig. 2 (a) Flowchart illustrating the literature classification process and (b) Sankey diagram showing the distribution and hierarchical relationships of published articles across three levels: publication journals, core dimensions, and subcategories.

raw literatures to structured knowledge, providing reliable data support and intelligent analytical tools for OPV research.

2.2. Literature Classification

The OPV research exhibits interdisciplinary characteristics due to its diverse material systems, complex device architectures, and multiscale physical mechanisms.[10,17,34] These lead to substantial variations in research focus and evaluation criteria across subfields. Uniform processing of literature data without proper differentiation would inevitably introduce interference. Therefore, we conducted literature classification to select studies directly relevant to molecular design while excluding confounding variables. This classification ensures the dimensional consistency and semantic alignment of extracted data. As shown in Fig. 2(a), the literature classification comprises two key stages: abstract extraction from literature images using multimodal large models (Fig. S1 in supporting information), and reliable zero-shot classification through domain knowledge-driven prompt engineering (PE). In the second stage, we designed a structured prompt template incorporating triple constraint mechanisms: (1) establishing a domain-specific classification system; (2) defining deterministic logic for classification decisions; (3) enforcing standardized JSON output format to enhance classification reliability (Fig. S2 in supporting information).

We constructed an OPV literature classification framework encompassing 7 core dimensions and 29 subcategories (Fig. 2(a)). The 7 core categories cover the entire innovation chain from molecular design to commercial applications, which strictly follows the "domain-technology" two-dimensional structure. The top-level dimensions classify different "domains" on key scientific and technological challenges—for instance,

View Article Online
DOI: 10.1039/D5EL00160A

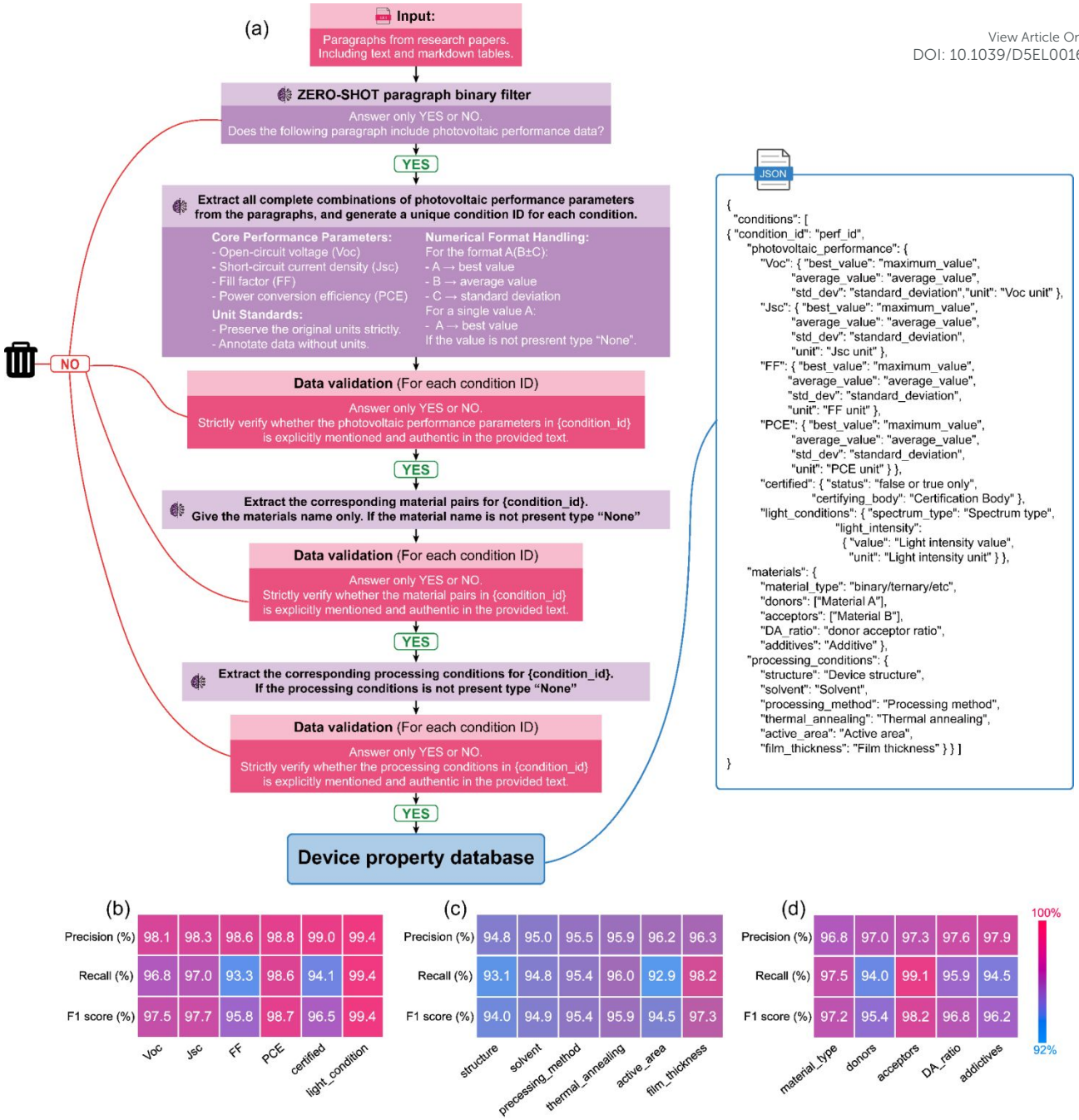

Fig. 3 (a) Flowchart illustrating the structured data extraction process. The average values of precision, recall, and F1 scores for 17 kinds of parameters in the extracted (b) device photovoltaic properties, (c) device processing conditions, and (d) material pairs.

material development and device physics address efficiency bottlenecks, while stability studies and application technologies target commercialization barriers. At the second level, research directions are categorized based on their technical relevance. Although each "technology" subfield is relatively independent, there are still interconnections among them. Thus, our classification system employs cross-references to reflect these synergistic relationships. This OPV literature classification framework not only establishes the interdisciplinary knowledge architecture for OPV, but also demonstrates outstanding adaptability to seamlessly incorporate future research progress.

Building on the classification framework, we analysed recent landscape of OPV research through a data-driven literature survey. We searched OPV research articles from Web of Science, using querying keywords "organic photovoltaics" and "organic solar cells" during 2019-2025 (starting from the landmark year of Y6). We initially randomly collected 615 peer-reviewed papers from multiple publishers including Wiley-VCH, American Chemical Society (ACS), Royal Society of Chemistry (RSC), and others (Fig. S3 in supporting information). We deployed the LLM Qwen2.5-VL-72b for structured abstract information extraction before utilizing DeepSeek-V3 for automatic literature classification. We visualized the literature

catalogues using Sankey diagram (Fig. 2(b)), which effectively represents flow relationships between hierarchical levels. The line width between nodes intuitively indicates the magnitude of the flow. The Sankey visualization reveals that our classification framework achieves broad coverage across all seven "core dimensions" and 25 out of 29 "subcategories". Nevertheless, at the higher levels of the hierarchy, all 615 papers are fully accounted for within the "core dimensions" and "subcategories" demonstrating the robustness, comprehensiveness, and systematic design of our classification framework. Within this well-structured catalogue, statistical analysis shows that 57.2% (358/615) of the publications focus on "Material development", making it the largest node among the core research dimensions. The category typically contains rich information on molecular design, physicochemical characterization, and structure–performance relationships. We thus prioritize in-depth analysis of this literature subset to systematically establish QMSPR for OPVs. Delving deeper, "Acceptor materials" emerges as the primary output pathway within "Material development," accounting for 53.1% (190/358) of publications, highlighting its pivotal role in advancing photovoltaic materials. The code for the framework is available on GitHub (https://github.com/limitedcommunication/Data-extraction).

2.3. Text Mining

After literature classification, we utilized the open-source LLM to extract the material and device data. The DeepSeek-V3 model was selected for two considerations: first, it enables localized data processing; second, it supports targeted model optimization. As illustrated in Fig. 3(a), the corresponding data extraction includes two steps—preliminary screening and data structuring. In the first step, domain knowledge-driven prompts help filter text paragraphs to effectively exclude irrelevant content. Then, multi-round progressive PE precisely extracts target data from the filtered paragraphs (Fig. S4 in supporting information). Following the framework, the DeepSeek-V3 model first identifies each set of the four critical photovoltaic parameters reported in the literature (open-circuit voltage (Voc), short-circuit current density (Jsc), fill factor (FF), and PCE) and then assigns a unique condition ID to each photovoltaic parameter set. Subsequently, the model associates each condition ID with the corresponding material pairs and device processing conditions, gradually constructing a complete experimental database. Benefiting from the standardized reporting conventions in OPV research (where most studies consistently report these four photovoltaic parameters), the risk of model-generated hallucination is substantially reduced. To ensure data reliability, we implemented a verification-feedback mechanism, where the LLM rechecks the original texts to confirm the existence of parameters and automatically triggers condition ID rematching upon detecting omissions. Notably, verification steps employ binary judgments (YES/NO) to control output length and enhance parsing efficiency. All outputs adhere to a predefined JSON schema, preserving both parameter values/units and hierarchical data structures (upper right panel of Fig. 3(a)).

To quantitatively evaluate the efficacy of structured data extraction, we established a benchmark dataset through triple cross-validation. 30 representative papers were randomly selected from the original literature corpus and independently annotated by domain experts to create a manual validation set. The evaluation employed a standardized framework to categorize each parameter extraction result into three types: true positive (TP, the model correctly identifies a parameter present in the manual annotation), false positive (FP, the model incorrectly identifies a parameter not present), and false negative (FN, the model fails to extract a reported parameter). The assessment strictly adhered to the data presence principle—only evaluating explicitly documented parameters to ensure unbiased results. As shown in Fig. 3(b), we calculated precision, recall, and F1 scores for 17 kinds of parameters (see the Methods section in supporting information for details). The system achieved overall metrics of precision 97.2±1.4%, recall 95.9±0.8%, and F1 score 96.6±1.1%. Collectively, these evaluation metrics highlight the effectiveness of the high-precision text mining methodology, demonstrating its capability to reliably transform unstructured scientific text into structured analysable data. Concurrently, we constructed a complete metadata framework containing literature identifiers including titles, digital object identifiers (DOIs), author information, abstracts, and publication years. The resulting OPV performance database ultimately incorporated over 47,000 structured data entries, providing a high signal-to-noise ratio foundation for subsequent analysis.

Combining the literature classification and device dataset, we gained clear insights into OPV research trends and performance evolution. Compared to traditional literature review approaches, this data-driven analytical paradigm provides a more objective and comprehensive depiction of the field's developmental trajectory. As the performance data statistics during 2019-2025 (Fig. S5 in supporting information), the reported champion PCE of binary systems rose from 16.5% to 20.8% accompanying with the average value markedly increasing from 11.2% to 17.4%.[1,5] The ternary material systems exhibited similar average PCE growth from 14.1% to 17.2% and champion value to the binary counterparts. The statistical results seem a bit contradict to the traditional views that the OPV devices based on ternary material systems have higher PCE values. Crucially, all high-performance devices—whether binary or ternary—relied on the incorporation of Y6 derivatives. The statistics unequivocally demonstrates the pivotal role of Y6 molecular scaffold innovation on driving OPV performance breakthrough.

2.3. QMSPR Construction

Building upon these analyses, we further elucidate the QMSPR between Y-series acceptors and their photovoltaic performances in OPV devices. Systematic understanding of this underlying correlation necessitates comprehensive and accurate extraction of electronic characteristics from molecular structures. We therefore developed an analytical framework incorporating HQCCP and explainable ML (Fig. 4(a)). The HQCCP integrates key components of molecular structure generation,

View Article Online
DOI: 10.1039/D5EL00160A

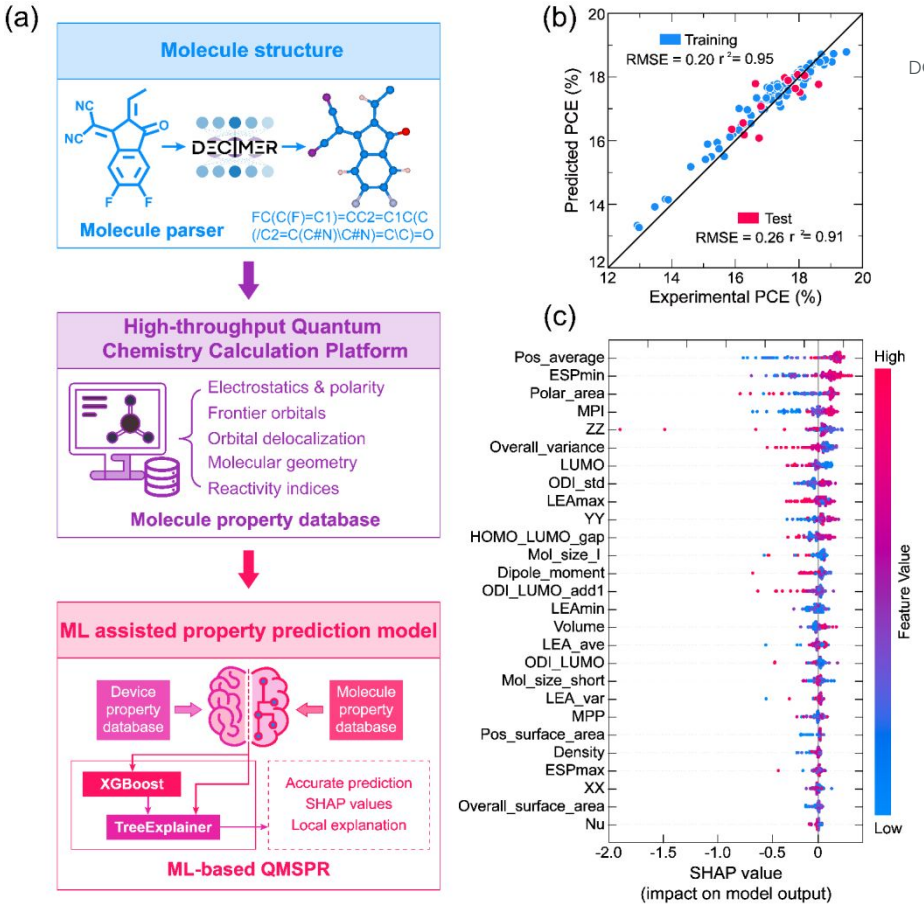

Fig. 4 (a) Overall schematic of the molecule parser, HQCCP, and explainable ML modules. (b) Predicted PCE by ML versus experimental PCE. (c) Illustration of features contributing to photovoltaic performances according to SHAP values of 27 molecular descriptors. Features on the right of the X-axis push the photovoltaic performances higher, and features on the left push them lower.

input file preparation, job scheduling, output parsing, and data storage into a unified workflow, which implements multi-level high-throughput quantum chemical calculations (Fig. S6 in supporting information, HQCCP software is available on GitHub: https://github.com/limitedcommunication/HQCCP). We employed the DECIMER package to convert 2D chemical structure images from literatures into SMILES strings, which were subsequently processed by HQCCP. The platform automatically analyses molecular structures and generates standardized input files using template engines. To balance computational efficiency with accuracy, HQCCP adopts a hierarchical calculation strategy: initial geometry optimization is performed using semi-empirical tight-binding (SE-TB) methods, followed by higher-level density functional theory (DFT) geometry optimization and single-point energy corrections based on pre-optimized structures. All quantum chemical calculations employ consistent parameter settings (including functionals and basis sets) to ensure comparability across different Y-series acceptors. The platform supports job submissions to local high-performance computing clusters with automated queue generation, featuring real-time monitoring, failure recovery, and error logging to significantly enhance computational stability and reliability. Upon completion, HQCCP automatically parses quantum chemical output files by Multiwfn, extracts key molecular descriptors, and stores them in standardized database formats (Fig. S6b in supporting information). The HQCCP systematically transforms implicit structural knowledge into 50 molecular descriptors, organized into five main categories: electrostatics and polarity, frontier orbitals, orbital delocalization, molecular geometry, and reactivity indices, further subdivided into 13 physically meaningful sub-categories (see Table S2 in supporting information for details). These descriptors comprehensively characterize the physicochemical properties of small molecule acceptors, which indicate the OPV device performance. We selected 125 representative Y-series acceptors from the literatures on "Materials development" catalogue obtained by the afore-mentioned classification (Table S3 in supporting information), spanning critical molecular engineering aspects. After computational analysis by HQCCP, we established the most comprehensive database of molecular descriptors for Y-series acceptors to date.

For each of these acceptors, we employed our HQCCP to compute a comprehensive set of 50 quantum-chemically derived molecular descriptors. To ensure the quality and independence of the input features, we conducted feature engineering with particular emphasis on redundancy analysis and dimensionality reduction among the 50 molecular descriptors. We first calculated the Pearson correlation coefficient matrix across all descriptors to identify the highly

View Article Online DOI: 10.1039/D5EL00160A

correlated feature pairs (Fig. S7 in supporting information). If the absolute correlation coefficient between two same sub-category descriptors exceeds 0.9, they are considered to convey redundant information. After screening, we selected 27 molecular descriptors that exhibited low multicollinearity and broad molecular informativeness (Table S2 in supporting information). The database was further integrated with the corresponding photovoltaic properties (PCE parameter), yielding a robust QMSPR dataset comprising a total of 125 × (27 descriptors + 1 PCE label) = 3500 distinct data points (The cleaned database is available on GitHub: https://github.com/limitedcommunication/Cleaned-dataset). Importantly, all machine learning tasks treat each molecule as a single sample represented by a 27-dimensional feature vector paired with one PCE value; thus, the effective sample size is 125. The 125 PCE values span a range of 12.7% to 19.78%, with a mean of 16.7% and a standard deviation of 1.9% (Fig. S8). Notably, approximately 28% of the entries exhibit PCE values below 15.7%—the benchmark efficiency reported for the Y6 molecule in its original publication. The PCE distribution demonstrating that the dataset encompasses not only state-of-the-art high-efficiency devices but also representative moderate- and lower-performance systems. This balanced distribution significantly enhances the reliability and generalizability of the subsequent ML analysis. However, it should be emphasized that this dataset, despite its performance spread, consists exclusively of published results and therefore reflects only the "survivor" molecules that demonstrated sufficient photovoltaic activity to warrant reporting. It does not include truly non-viable candidates that failed during synthesis, processing, or basic device operation. Consequently, the model is best suited for guiding molecular refinement and optimization within the established chemical space of Y-series non-fullerene acceptors, rather than for screening arbitrary structures or identifying fundamentally non-functional materials.

Based on the constructed QMSPR dataset, we developed a ML model for predicting OPV device performance using the XGBoost algorithm.[36,37] The model was integrated with the SHAP framework—a cooperative game theory-based interpretability tool—to enable transparent and interpretable predictions (Fig. 4(a)).[38,39] The complete dataset was partitioned into training and independent test sets at a 90%-10% ratio. To optimize model parameters and ensure predictive performance, we conducted an exhaustive grid search of key XGBoost hyperparameters through 5-fold cross-validation within the training set. The optimized model achieved a root mean square error (RMSE) of 0.26 and a coefficient of determination (r^2) of 0.91 on the independent test set, demonstrating robust prediction accuracy (Fig. 4(b)). The Comparable performance on the training set (RMSE = 0.24, r^2 = 0.95) indicates that the model effectively learned the underlying structure of the data without significant overfitting (XGBoost framework code is available on https://github.com/limitedcommunication/OPV_analyzer). To rigorously evaluate the generalization capability of our model, we performed a prospective validation on L8-BO-X, a Y-series NFA not included in the original 125-molecule set. For the binary blend PM6:L8-BO-X (1:1.2), the experimentally measured PCE is 17.56% (Fig. S9, validation code is available on: https://github.com/limitedcommunication/L8-BO-X_validation).[40] Using our HQCCP, we computed the same 27 quantum-chemical descriptors used in model training and standardized them with the training-set scaler. When input into the frozen XGBoost model, L8-BO-X yielded a predicted PCE of 17.55%, corresponding to an absolute error of just 0.01%. This result further supporting the generalizability and predictive reliability of our model. Building upon this well-trained model, we implemented the game theory-based SHAP analysis to quantitatively assess each feature's contribution. This approach provides a unified metric that not only ranks feature importance but also reveals their influences on predictions. It is important to note that the predicted PCEs represent an upper-bound estimate of a molecule's performance potential, contingent upon processing conditions. Consequently, the molecular design rules derived from our model should be interpreted as guidelines for molecular engineering within high-performance OPV systems, rather than universal guarantees of device efficiency under arbitrary fabrication protocols. This distinction underscores that our framework captures the interplay between molecular structure and achievable performance under ideal processing, not intrinsic performance independent of processing. It should be noted that the current evaluation relies on a random train–test split, which may inadvertently allow structurally similar molecules to appear in both sets, potentially overestimating predictive performance. While scaffold- or time-based splitting strategies would provide a more rigorous assessment of generalization to truly novel chemistries, the limited size and scope of the present dataset constrain the feasibility of such approaches.

SHAP-based visualization reveals key predictive features for OPV performance and their underlying mechanisms (Fig. 4(c) and Fig. S10 in supporting information). Quantitative feature importance analysis reveals that the "Electrostatic & polarity" descriptors dominate PCE prediction, accounting for a cumulative contribution of 63.1%. Among these, Pos_average (average positive electrostatic potential) exhibits the highest contribution (12.6%), followed by ESPmin (minimum electrostatic potential, 11.0%), Polar_area (polar surface area, 8.8%), and the MPI (molecular polarity index, 7.0%). SHAP value analysis also confirms that increased values of these descriptors correlate strongly with higher PCE, suggesting that enhancing the four "Electrostatic & polarity" descriptors above improves device performance. Notably, the ZZ component of molecular quadrupole moment ranks as the fifth most important feature, with a contribution of 6.7%. Different from the former four features, it negatively impacts PCE. This finding appears to contradict with some earlier reports where larger ZZ values were generally shown to improve device performance by promoting charge separation through increased D-A interfacial potential differences.[42,43] Importantly, existing studies also indicate that the ZZ component can influence molecular packing behaviour.[41] We therefore propose that the net effect of ZZ component of molecular quadrupole moment on PCE likely

View Article Online
DOI: 10.1039/D5EL00160A

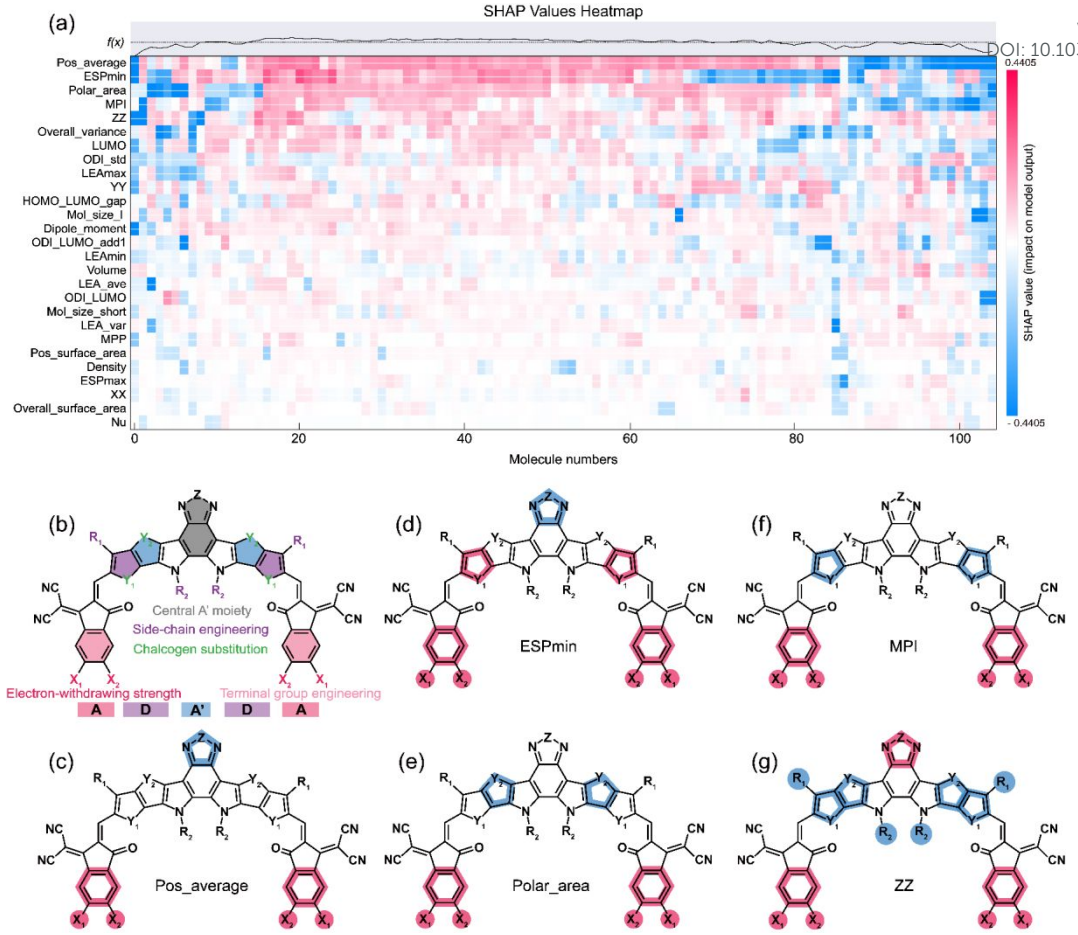

Fig. 5 (a) SHAP values heatmap illustrating the contribution of molecular descriptors to model predictions across 125 molecules. Each column represents an individual molecule, and each row corresponds to a molecular descriptor. The colour intensity (blue to red) indicates the direction and magnitude of each feature's impact on the model output, with red denoting positive contributions and blue indicating negative contributions. The top panel shows the predicted output f(x) , reflecting variation in performance across molecules. (b) Basic structure of A–DA'D–A type Y-series acceptor and corresponding molecular engineering strategies. The labels X_1, X_2, Y_1, Y2, and Z highlight structural diversity. X_1 and X_2 represent terminal substituent atoms (e.g., F, Cl, Br) at the terminal groups, which may be identical or different. Y_1 and Y2 denotes substituents on the D unit, typically S or Se atoms; when identical, no subscript is used. Z represents substituent atoms on the A' unit, potentially including S or Se atoms. Analysis of the relationship between different molecular fragments and (c) Pos_average, (d) ESPmin, (e) Polar_area, (f) MPI, and (g) ZZ using the XGBoost model combined with SHAP.

represents a trade-off between its beneficial interfacial electrostatic effects and potential morphological drawbacks. Given the electronic significance of ZZ and the non-intuitive trend revealed here, the multifaceted role of this component warrants further studies.

For deeper insight into the model's decision-making at the individual molecule level, we visualized SHAP values in a heatmap format (Fig. 5(a)): 125 columns represent 125 distinct molecules in the dataset, and each row corresponds to a molecular descriptor. This representation reveals the direction and magnitude of each feature's contribution to the prediction for individual molecules. Notably, while some molecules exhibit strong and consistent contributions from specific descriptors, others display more complex, multi-feature interaction patterns, highlighting the heterogeneity in molecular behaviour. This per-molecule analysis provides a transparent and interpretable view of the model's internal logic. It demonstrates that the model does not rely on uniform feature importance but instead adapts its reasoning based on the unique chemical profile of each acceptor.

To further elucidate the structural origins of key molecular descriptors, we tried to associate these descriptors with specific molecular blocks to build QMSPR for Y-series acceptors. We utilize Extended-Connectivity Fingerprints (ECFP) (see calculation details in Method and Fig. S11 in supporting information) to include the chemical information of local environment in molecular strings.[6,30,31,44] ECFP does not treat molecules as simple strings; instead, it systematically identifies circular topological neighbourhoods around each atom and hashes them into a fixed-length binary vector. Each bit represents the presence or absence of a specific substructural motif. This representation allows ML models to capture complex functional groups and their spatial contexts in a numerically tractable format. By recognizing topological neighbourhoods around each atom and encoding them into fixed-length binary vectors, ECFP efficiently captures

information on functional groups and their spatial arrangements. These ECFP fingerprints are subsequently used to map molecular structures to five target descriptors: Pos_average, ESPmin, Polar_area, MPI, and ZZ. Using the XGBoost, we construct high-performance predictive models, achieving R^2 of 0.82, 0.95, 0.81, 0.79, and 0.83 on the independent test set, respectively (Fig. S12 in supporting information). These results indicate a reliable relationship between the ECFP fingerprints and key molecular descriptors. To dissect the specific contributions of molecular substructures to each descriptor, we apply SHAP analysis to all five models (Fig. 5(b-g) and Table S4 in supporting information). SHAP analysis reveals a positive correlation between the end groups and all five molecular descriptors. Specifically, as the electron-withdrawing capacity of the end groups increases, all molecular descriptors exhibit an upward trend. Through quantitative model evaluation, we conclusively demonstrate that although the ZZ component shows a negative correlation with PCE, the weighted contribution of the end groups to the device PCE remains positive, accounting for 11.3%. This result indicates that enhancing the electron-withdrawing ability of the end groups can effectively improve the device's PCE. Further analysis reveals that the benzothiadiazole (BTD) core in Y-series acceptors exhibits a significant negative correlation with two key electrostatic potential descriptors (Pos_average and ESPmin) while showing a positive correlation with ZZ. Ultimately, the electron-withdrawing capacity of the BTD core negatively correlates with PCE, with a contribution of -8.7%. Additionally, the donor (D) units in these molecules exhibit a somewhat contradictory influence on electrostatic potential-related descriptors (ESPmin and MPI), suggesting the presence of a nonlinear regulatory mechanism affecting local charge distribution. In contrast, the D units display a clear negative correlation with the ZZ descriptor (Fig. 5(g)). Quantitative analysis further reveals that enhancing the electron-donating ability of the D units contributes to improving the device's power conversion efficiency (PCE), with a quantified contribution of 0.1%. Notably, side-chain engineering demonstrates a pronounced negative correlation with the ZZ descriptor (Fig. 5(g)). This indicates that increasing the bulkiness of the outer alkyl chains and introducing functionalized substituents on the inner side can enhance device PCE, with an overall contribution of 2.7%. As visualised in Fig. S13, it not only confirms the structural consistency of this motif across diverse molecular scaffolds but also reveals its atomic-level specificity: the bit is activated by multiple central atoms within the same fluorinated aromatic ring, each contributing to the overall positive SHAP value. The slight variation in SHAP magnitude (+0.4017 vs. +0.3917) between molecules suggests that while the core substructure is universally beneficial, its exact chemical environment can modulate its impact on PCE. This level of granularity linking a single fingerprint bit to specific atom environments and quantifying their individual contributions, which is precisely what enables our model to provide actionable, chemically interpretable design rules.

Based on these findings, we propose the following design guidelines for Y-series acceptors. First, strong electron-withdrawing end groups are prioritized to significantly improve PCE. Second, while maintaining the conjugated core framework, excessive electron-withdrawing strength at the central A' core should be avoided. Third, D units should be designed with moderate electron-donating capability to prevent PCE reduction from overly strong donating effects. Finally, side-chain engineering requires precise spatial control for optimal device performance. Collectively, high-performance acceptors should adopt a "strong ends, stable core, moderate donor, controlled side chains" optimization strategy to achieve systematic device improvement through synergistic molecular design. All molecular design guidelines derived from SHAP analysis should be interpreted as testable hypotheses generated from statistical patterns in the data, not as established physical laws. Experimental synthesis and device characterization remain essential to confirm causality and assess practical viability. The primary utility of our framework lies in high-throughput virtual screening and relative ranking of candidate molecules within the chemical space spanned by known Y-series acceptors, rather than in predicting absolute PCEs for unprecedented, record-breaking materials. The model excels at identifying promising structural motifs and filtering out low-performing candidates, tasks that significantly accelerate early-stage discovery. However, absolute PCE predictions for top-tier performers should be treated with caution.

2.4. Applicability Domain and Generalization Potential

The machine learning framework presented in this work is trained and validated exclusively on a dataset of 125 Y-series non-fullerene acceptors, which share a common molecular architecture featuring a fused-ring electron-donating core, electron-withdrawing end groups, and solubilizing side chains. Consequently, the derived structure–property relationships are specific to this chemical family and should not be extrapolated to structurally distinct acceptor classes without validation. The applicability domain of our model is thus defined by the chemical and topological similarity to known Y-series scaffolds. It is well-suited for virtual screening and molecular optimization within this established space, but it cannot reliably predict the performance of molecules that deviate significantly in core topology, conjugation length, or electronic motif.

To extend this framework to other photovoltaic material classes, several key steps are required:

(1) Construct category-specific datasets with unified device structures and champion PCE values;

(2) Develop or adapt molecular descriptors to capture the key physical properties of the new material systems;

(3) Retrain or fine-tune the machine learning model using the new data.

Major challenges include the scarcity of standardized data for emerging material classes and the need for descriptors that generalize across diverse chemical motifs. Nevertheless, the modular architecture of our framework: combining LLM-based literature mining, quantum-chemical computation, and explainable ML. Which provides a scalable foundation for such extensions. Future work will focus on adapting this pipeline to polymer donors, all-polymer systems, and tandem cell subcells,

thereby advancing toward a universal data-driven platform for organic photovoltaics.

3. Conclusions

In summary, this study establishes a robust high-throughput computational and analytical pipeline tailored for the OPV field and advances the understanding of the structure–property relationships in Y-series NFA molecules. We developed an IDDF that combines LLM-powered knowledge extraction, HQCCP, and explainable ML. This framework adopts a data-driven approach to accelerate materials innovation. We curated a comprehensive dataset comprising 615 peer-reviewed articles and calculated 27 molecular descriptors for 125 Y-series acceptors. This enabled the construction of a robust QMSPR database that links molecular substructures with multiple descriptors to device performances, establishing a solid data foundation for model training and analysis. On this basis, our explainable XGBoost-SHAP ML model achieves accurate predictions of device performance and quantifies the impact of molecular substructures. The framework represents a step toward replacing the slow and heuristic development of OPV materials with a systematic and computationally efficient approach. The methodology also provides a scalable pathway for advancing high-performance and sustainable energy materials.

Author Contributions

H.Y. proposed and supervised the project. Y.C. designed and implemented the calculation platform, developed the explainable machine learning models, and constructed the large language model pipeline for literature data extraction. Y.C. and H.Y. co-authored the paper. All authors discussed the results and participated in the analysis.

Conflicts of interest

There are no conflicts to declare.

Acknowledgements

This work was supported by the National Natural Science Foundation of China (22475164) and the S&T Program of Energy Shaanxi Laboratory, Grant No. ESLB202440. This work was also supported by the following artificial intelligence technologies: Qwen2.5-72B, Qwen2.5-VL-72B, and DeepSeek-V3. These open-source large language models were employed to analyse textual content, tables, and figures for information extraction and literature classification.

Notes and references

1 J. Yuan, Y. Zhang, L. Zhou, G. Zhang, H.-L. Yip, T.-K. Lau, X. Lu, C. Zhu, H. Peng, P. A. Johnson, M. Leclerc, Y. Cao, J. Ulanski, Y. Li and Y. Zou, *Joule*, 2019, **3**, 1140-1151.
2 Y. Jiang, S. Sun, R. Xu, F. Liu, X. Miao, G. Ran, K. Liu, Y. Yi, W. Zhang and X. Zhu, *Nat. Energy*, 2024, **9**, 975–986.
3 C. Chen, L. Wang, W. Xia, K. Qiu, C. Guo, Z. Gan, J. Zhou, Y. Sun, D. Liu, W. Li and T. Wang, *Nat. Commun.*, 2024, **15**, 6865.
4 J. Fu, Q. Yang, P. Huang, S. Chung, K. Cho, Z. Kan, H. Liu, X. Lu, Y. Lang, H. Lai, F. He, P. W. K. Fong, S. Lu, Y. Yang, Z. Xiao and G. Li, *Nat. Commun.*, 2024, **15**, 1830.
5 C. Li, Y. Cai, P. Hu, T. Liu, L. Zhu, R. Zeng, F. Han, M. Zhang, M. Zhang, J. Lv, Y. Ma, D. Han, M. Zhang, Q. Lin, J. Xu, N. Yu, J. Qiao, J. Wang, X. Zhang, J. Xia, Z. Tang, L. Ye, X. Li, Z. Xu, X. Hao, Q. Peng, F. Liu, L. Guo and H. Huang, *Nat. Mater.*, 2025, DOI: 10.1038/s41563-025-02305-8.
6 C. Li, J. Song, H. Lai, H. Zhang, R. Zhou, J. Xu, H. Huang, L. Liu, J. Gao, Y. Li, M. H. Jee, Z. Zheng, S. Liu, J. Yan, X.-K. Chen, Z. Tang, C. Zhang, H. Y. Woo, F. He, F. Gao, H. Yan and Y. Sun, *Nat. Mater.*, 2025, **24**, 433–443.
7 J. Ding, H. Mou, H. Chen, J. Xu, W. Sun, J. Zhu, Y. Wang, Y. Huang, Y. Li and Y. Li, *Adv. Mater.*, 2025, **37**, 20240439.
8 H. Liang, X. Bi, H. Chen, T. He, Y. Lin, Y. Zhang, K. Ma, W. Feng, Z. Ma, G. Long, C. Li, B. Kan, H. Zhang, O. A. Rakitin, X. Wan, Z. Yao and Y. Chen, *Nat. Commun.*, 2023, **14**, 4707.
9 J. Yi, G. Zhang, H. Yu and H. Yan, *Nat. Rev. Mater.*, 2023, **9**, 46-62.
10 N. Yang, S. Zhang, Y. Cui, J. Wang, S. Cheng and J. Hou, *Nat. Rev. Mater.*, 2025, **10**, 404-424.
11 Y. Tang, Y. Cui, R. Zhang, W. Xue, W. Ma and H. Yan, *Adv. Energy Mater.*, 2024, **14**, 2303799.
12 F. Xue, Y. Xie, Y. Cui, D. Y. Paraschuk, W. Ma and H. Yan, *Adv. Funct. Mater.*, 2024, **35**, 2415617.
13 K. Zhou, D. Han, K. Xian, S. Li, M. Gao, K. Zhang, B. Zhao, X. Li, Y. Chen, Y. Geng and L. Ye, *Energy Environ. Sci.*, 2024, **17**, 5950-5961.
14 Z. Wang, D. Zhang, L. Yang, O. Allam, Y. Gao, Y. Su, M. Xu, S. Mo, Q. Wu, Z. Wang, J. Liu, J. He, R. Li, X. Jia, Z. Li, L. Yang, M. D. Weber, Y. Yu, X. Zhang, T. J. Marks, N. Stingelin, J. Kacher, S. S. Jang, A. Facchetti and M. Shao, *Science*, 2025, **387**, 381-387.
15 S. Lee, S. Oh, S. Han, D. Lee, J. Lee, Y. Kim, H.-Y. Jeong, J.-W. Lee, M.-H. Lee, W. B. Ying, S. Jeong, S. Lee, J. Kim, Y. H. Kim, B. J. Kim, E.-c. Jeon, T.-S. Kim, S. Cho and J.-Y. Lee, *Energy Environ. Sci.*, 2024, **17**, 8915-8925.
16 J.-W. Lee, H.-G. Lee, E. S. Oh, S. W. Lee, T. N.-L. Phan, S. Li, T.-S. Kim and B. J. Kim, *Joule*, 2024, **8**, 204-223.
17 J. Wang, Y. Xie, K. Chen, H. Wu, J. M. Hodgkiss and X. Zhan, *Nat. Rev. Phys.*, 2024, **6**, 365-381.
18 X. Li, M. Cui, J. Li, R. Bai, Z. Lu and U. Aickelin, *Neurocomputing*, 2021, **443**, 345-355.
19 T. Gupta, M. Zaki, N. M. A. Krishnan and Mausam, *npj Comput. Mater.*, 2022, **8**, 102.
20 H. Huang, R. Long, H. Chen, K. Sun and Q. Li, *Sustain. Prod. Consum.*, 2022, **30**, 674-685.
21 T. Brown, B. Mann, N. Ryder, M. Subbiah, J. D. Kaplan, P. Dhariwal, A. Neelakantan, P. Shyam, G. Sastry, A. Askell, S. Agarwal, A. Herbert-Voss, G. Krueger, T. Henighan, R. Child, A. Ramesh, D. M. Ziegler, J. Wu, C. Winter, C. Hesse, M. Chen, E. Sigler, M. Litwin, S. Gray, B. Chess, J. Clark, C. Berner, S. McCandlish, A. Radford, I. Sutskever and D. Amodei, *Adv. Neural. Inf. Process. Syst.*, 2020, **33**, 1877.
22 A. Vaswani, N. Shazeer, N. Parmar, J. Uszkoreit, L. Jones, A. N. Gomez, Ł. Kaiser and I. Polosukhin, *Adv. Neural. Inform. Process. Syst.*, 2017, **30**.
23 Z. Zheng, O. Zhang, C. Borgs, J. T. Chayes and O. M. Yaghi, *J. Am. Chem. Soc.*, 2023, **145**, 18048-18062.
24 Y. Kang and J. Kim, **Nat. Commun.**, 2024, **15**. 4705.
25 M. P. Polak and D. Morgan, *Nat. Commun.*, 2024, **15**, 1569.
26 Y. Kang, W. Lee, T. Bae, S. Han, H. Jang and J. Kim, *J. Am. Chem. Soc.*, 2025, **147**, 3943-3958.

View Article Online
DOI: 10.1039/D5EL00160A

27 J. Ross, B. Belgodere, V. Chenthamarakshan, I. Padhi, Y. Mroueh and P. Das, *Nat. Mach. Intell.*, 2022, **4**, 1256-1264.
28 X. Zeng, H. Xiang, L. Yu, J. Wang, K. Li, R. Nussinov and F. Cheng, *Nat. Mach. Intell.*, 2022, **4**, 1004-1016.
29 P. Bai, F. Miljković, B. John and H. Lu, *Nat. Mach. Intell.*, 2023, **5**, 126-136.
30 G. Han and Y. Yi, *Angew. Chem. Int. Ed.*, 2022, **61**, e202213953.
31 S. Liu, D. Zhang, H.-J. Egelhaaf, G. Wang, X. Li, T. Heumüller, C. J. Brabec and N. Li, *J. Mater. Chem. A.*, 2024, **12**, 14688-14697.
32 L. Zhu, M. Huang, G. Han, Z. Wei and Y. Yi, *Angew. Chem. Int. Ed.*, 2025, **64**, e202413913.
33 S. Shahzadi, T. Shahzadi, Z. Shafiq and Muhammad Ramzan Saeed Ashraf Janjua, High Energy Chem., 2024, **58**, 583–603.
34 J. Dagdelen, A. Dunn, S. Lee, N. Walker, A. S. Rosen, G. Ceder, K. A. Persson and A. Jain, *Nat. Commun.*, 2024, **15**, 1418.
35 J. Luke, E. J. Yang, C. Labanti, S. Y. Park and J.-S. Kim, *Nat. Rev. Mater.*, 2023, **8**, 839-852.
36 T. Chen and C. Guestrin, *in Proceedings of the 22nd ACM SIGKDD International Conference on Knowledge Discovery and Data Mining*, Association For Computing Machinery, San Francisco 2016.
37 Y. Cui, Q. Fan, H. Feng, T. Li, D. Y. Paraschuk, W. Ma and H. Yan, *Energy Environ. Sci.*, 2024, **17**, 8954-8965.
38 S. M. Lundberg, B. Nair, M. S. Vavilala, M. Horibe, M. J. Eisses, T. Adams, D. E. Liston, D. K.-W. Low, S.-F. Newman, J. Kim and S.-I. Lee, *Nat. Biomed. Eng.*, 2018, **2**, 749-760.
39 S. M. Lundberg, G. Erion, H. Chen, A. DeGrave, J. M. Prutkin, B. Nair, R. Katz, J. Himmelfarb, N. Bansal and S.-I. Lee, *Nat. Mach. Intell.*, 2020, **2**, 56-67.
40 J. Song, C. Zhang, C. Li, J. Qiao, J. Yu, J. Gao, X. Wang, X. Hao, Z. Tang, G. Lu, R. Yang, H. Yan and Y. Sun, Angew. Chem. Int. Ed., 2024, **63**, e202404297.
41 K. Yamada, S. Yanagisawa, T. Koganezawa, K. Mase, N. Sato and H. Yoshida, *Phys. Rev. B*, 2018, **97**, 245206.
42 M. Schwarze, C. Gaul, R. Scholz, F. Bussolotti, A. Hofacker, K. S. Schellhammer, B. Nell, B. D. Naab, Z. Bao, D. Spoltore, K. Vandewal, J. Widmer, S. Kera, N. Ueno, F. Ortmann and K. Leo, *Nat. Mater.*, 2019, **18**, 242-248.
43 S. Y. Park, C. Labanti, R. A. Pacalaj, T. H. Lee, Y. Dong, Y. C. Chin, J. Luke, G. Ryu, D. Minami, S. Yun, J. I. Park, F. Fang, K. B. Park, J. R. Durrant and J. S. Kim, *Adv. Mater.*, 2023, **35**, 2306655.
44 D. Rogers and M. Hahn, *J. Chem. Inf. Model.*, 2010, **50**, 742.

Data available within the article or its supplementary Information.

View Article Online
DOI: 10.1039/D5EL00160A